De-convolution based correction of alkali beam emission spectroscopy density profile measurements

I. Pusztai[1], G. Pokol[2], D. Dunai[3], D. Réfy[2], G. Pór[2], G. Anda[3], S. Zoletnik[3], J. Schweinzer[4]

[1] *Department of Radio and Space Science, Chalmers University of Technology and Euratom-VR Association, SE-41296 Göteborg, Sweden*

[2] *Department of Nuclear Techniques, Budapest University of Technology and Economics, Association EURATOM, Műegyetem rkp. 9., H-1111 Budapest, Hungary*

[3] *KFKI-RMKI, Association EURATOM, Pf. 49, H-1525 Budapest, Hungary*

[4] *Max-Planck-Institut für Plasmaphysik, Association EURATOM, D-85748 Garching, Germany*

July 21, 2009

Abstract

A de-convolution based correction method of the beam emission spectroscopy density (BES) profile measurement is demonstrated by its application to simulated measurements of the COMPASS and TEXTOR tokamaks. If the line of sight is far from tangential to the flux surfaces, and the beam width is comparable to the scale length, on which the light profile varies, the observation may cause an undesired smoothing of the light profile, resulting in a non-negligible underestimation of the calculated density profile. This effect can be reduced significantly by the *emission reconstruction method* which gives an estimate of the emissivity along the beam axis, from the measured light profile, taking the finite beam width and the properties of the measurement into account in terms of the transfer function of the observation. Characteristics and magnitude of the mentioned systematic error and its reduction by the introduced method are studied by means of the comprehensive alkali BES simulation code RENATE.

1

1 Introduction

Lithium Beam Emission Spectroscopy (Li-BES) is an active diagnostic tool, typically probing the outer regions of fusion plasmas by observing the characteristic emission of a 10–100 keV atomic beam injected into the plasma [1, 2]. Li-BES measurements are routinely performed on several fusion devices [3]. Application of sodium for BES purposes is recently considered [4, 5], thus we refer the method as *alkali BES* hereafter.

The evolution of the populations of different atomic states depends on the distribution of plasma parameters along the beam line. This means that from the emitted intensity distribution at a characteristic frequency (i.e. the *light profile*) information can be obtained on the distribution of electron density [6] and its fluctuation [2].

Advantages of the alkali BES diagnostic include being practically non-intrusive – because of the low density of the beam, – and being approximately a point measurement. The technique is exceedingly suitable for Scrape-Off Layer (SOL) and pedestal density profile measurements with good temporal and spatial resolution (50 μs, 5 mm [7]), thus contributes to the understanding of transitions between different confinement modes and to the validation of models of edge transport barrier formation [8]. Statistical behavior of density fluctuations with $\sim \mu$s time scale in the edge and SOL (e.g. radial wave number spectra, correlation length and time) can also be investigated in the radial direction by "single beam" fluctuation measurements [2]. Moreover, fluctuation measurements can be extended to two dimensions by electrostatically deflecting the beam in the poloidal plane in the fluctuation's time scale in order to obtain a complex picture of the cross field turbulent transport [9]. We have to point out that the high temporal resolution fluctuation measurements need always to be combined with the significantly slower profile measurement.

The *collisional-radiative model* is considered in the standard description of beam evolution [10]. Based on this model, reliable numerical methods were developed to determine the density profiles along the beam line, given the observed light profile [7, 11, 12], such as the Li-BES density reconstruction code, Absolut, which is used in the present

study [6]. All these methods are based on the assumption that the measured light profile is equivalent to the emissivity of the beam. This case corresponds to the *ideal* measurement geometry considering the beam to be one dimensional and neglecting its finite width.

Our goal is to provide a tool to quantitatively measure the systematic error caused by this simplified treatment. Partially for this purpose, as well as to support the design and interpretation of BES measurements, the RENATE alkali BES simulation code has been developed. For the purpose of this study, alkali BES set-up and plasma parameters are chosen from the recently upgraded TEXTOR Li-BES diagnostic [13], and the alkali BES diagnostic planned for the newly restarted COMPASS [14]. We investigate the character and magnitude of the systematic error in density profile reconstruction, and conclude that it can be significant in certain, experimentally relevant cases, which we support with a general estimation of the maximal error in the calculated electron density. The simulation of the phenomenon also enabled the design of a method for the correction of the measured light profile reducing the effect of the finite beam width, and thus allowing the use of the one dimensional density reconstruction methods.

The structure of the paper is as follows: In Sec. 2 the of the alkali BES measurement simulation, RENATE is introduced. The issues of the observation of a finite width beam are investigated in Sec. 3. The emission reconstruction correction method is discussed in Sec. 4, and demonstrated through realistic simulated measurements in Sec. 5. A general estimate of the error due to finite beam width is given in Sec. 6, and finally, the results are summarized in Sec. 7.

2   RENATE alkali BES measurement simulation

For the purpose of supporting the design of alkali BES density profile and fluctuation measurements, an IDL language simulation code, RENATE, has been developed which also assists the interpretation and correction of measured data. In order to take the finite width of the beam into account the beam evolution is calculated separately in slices of the

beam considering a realistic current distribution. The integration of emitted light along the lines of sight is modeled together with other essential features of the observation and the detector system.

The atomic physics processes of the beam are modeled by the *collisional radiative model* [10]. The *rate equations* describing the evolution of atomic occupations can be written in a quite compact form

$$\frac{dn_i}{dx} = \sum_j \left[n_e(x)\tilde{a}_{ij}(x) + b_{ij} \right] n_j(x) \qquad (i,j = 1, \cdots, m), \tag{1}$$

where n_e is the electron density, n_i and n_j are populations of the ith and j^{th} atomic states respectively and x is the coordinate along the beam. The atomic transition and electron loss processes due to electron (e), proton (p) and impurity (I) collisions are described by the reduced rate coefficient matrix $\tilde{a}_{ij}$ [4, 15, 16, 17]. Taking the effect of the impurities into account through one representative impurity characterized by charge $q(x)$ and producing an effective ion charge $Z_{eff}(x)$, the matrix is written as $\tilde{a}_{ij} = a_{ij}^e + (1 - qf)a_{ij}^p + fa_{ij}^I$, where $f = (Z_{eff} - 1)/(q(q-1))$. The spontaneous atomic transitions are described by the b_{ij} matrix. In the simulation the number of registered atomic levels are $m = 9$ for lithium and $m = 7$ for sodium. Note that $\tilde{a}_{ij}$ depends on x not only through q and Z_{eff} but due to the temperature dependence of the rate coefficients. The ion and impurity temperatures are chosen to be equal to the electron temperature, causing only a negligibly small error, due to the flat temperature dependence of a_{ij}^p and a_{ij}^I.

The photon emission density of a beam per unit time and length is proportional to $n_\iota I A_{\varphi\iota}/v_B$, where the observed spectroscopic line corresponds to the $\iota \to \varphi$ transition ($2p \to 2s$ for Li, $3p \to 3s$ for Na), v_B is the beam velocity, $A_{\varphi\iota}$ is the corresponding Einstein coefficient and I is the beam current. The n_ι population is calculated by the solution of the *direct problem*, integrating equation (1) stepwise from the point where the beam enters into the plasma $x = 0$, with the initial condition $n_i(0) = \delta_{i1}$, where 1 is the index of the ground state.

Since the RENATE code was originally developed with the purpose of design of BES

measurements, it solves the direct problem calculating the beam evolution and the emission distribution for a given measurement configuration and set of plasma parameters. Therefore, the most important component of the simulation is its *atomic physics kernel*, which calculates the rate coefficients from parametrically given cross sections of the collisional processes and solves the rate equations (1) by a 4$^{\text{th}}$ order Runge-Kutta method. The spontaneous atomic transition probabilities are taken from the NIST atomic spectra database [18], and the cross section data found in [15, 16, 17] for lithium and [4] for sodium are used. The collisional $j \to i$ de-excitation rate coefficients are derived from the corresponding $i \to j$ excitation rate coefficients using the principle of detailed balance, while impurity collision rate coefficients are calculated from the proton collisional cross sections using the scaling relations given in [4, 15]. The proton impact target electron loss processes are considered instead of treating the ionization and charge exchange channels separately, which is the main difference of the atomic physics kernel from the Absolut [6] inverse problem solver regarding the atomic physics.

Absolut has a corresponding direct solver code called Simula, which we used for the validation of RENATE; the found relative difference between the rate coefficients calculated by the different programs is $\mathcal{O}(10^{-4})$, and accordingly the maximum relative difference between the calculated evolution of atomic populations is the same order of magnitude. The Absolute code in turn has been critically tested against both Li [6] and Na [5] measurements. In this manner, RENATE is indirectly validated to measurements; the direct validation is under way at the TEXTOR tokamak.

The calculation scheme of the simulation is as follows. First, the beam is divided into slices which are perpendicular to the poloidal plane while the velocity of the beam atoms is tangential to them. The emissivity profile is calculated along each slice, given the magnetic geometry $\Psi(R, Z)$, together with the distribution of the relevant plasma parameters, n_e, T_e, q and Z_{eff} as a function of a flux coordinate Ψ. The plasma parameters are assumed to be equally distributed on a flux surface. Then the calculation of the *geometric efficiency* (i.e. the effect of that the collecting optical element covers different solid angles seen from

5

different points of the beam) is performed for the points of each slice, and the efficiency of the observation system is taken into account in order to determine the number of photons per unit time detected by each detector segment. Contributions of the different beam slices and points to the detected signal are summed up.

We restrict our studies to measurement geometries where the beam axis is in the poloidal plane and the "observation point" is also located in the same toroidal position, which is typical for diagnostic neutral beams. In this case, we can project the three dimensional beam into the poloidal plane of the beam axis, and the observed volumes reduce to observed areas.

3 Observation of a finite width beam

Observing the emission of a diagnostic beam means integrating the emissivity along the lines of sight weighted by the geometric efficiency. Since the beam has a finite width, a line of sight goes through parts of the beam being in different stages of beam evolution, thus the measurement cannot be perfectly local. Inverting this effect, the emission reconstruction method gives an estimate of the emissivity on the beam axis from a measured light profile.

We denote the coordinate measured along the beam axis by x, and index each segment of the detector array by x' marking the position where the middle of the observed volume of the detector segment intersects the beam axis (see Fig. 1). For the sake of simplicity of the formalism, x' is also considered to be a continuous independent variable.

Assuming that the plasma parameters are flux functions, it can be concluded from our simulations that the evolution of atomic populations also follows the flux surfaces, except from extreme cases of wide beams injected almost tangentially to the flux surfaces. This enables us to extend the emissivity along the beam axis $I(x)$ into two dimensions by mapping along the flux surfaces indexed by x'' marking their intersection with the beam axis and weighting with the beam current distribution. Thus, we can express the

measured light profile $S(x')$ as

$$S(x') = \int T(x', x)I(x)\mathrm{d}x, \tag{2}$$

where the kernel function $T(x', x)$ is called the *transfer function of the observation*. Obviously, the goal is to determine $I(x)$ from a measured $S(x')$.
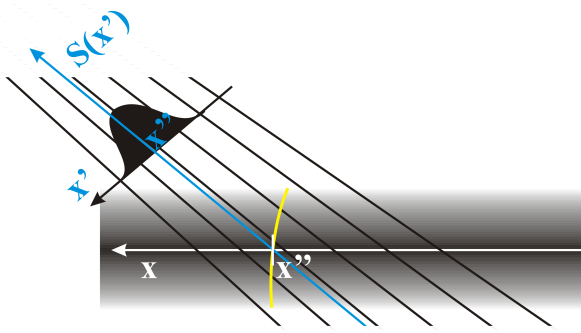

Figure 1: Construction of the transfer function of the observation. x is the coordinate along the beam axis, which is one-to-one mapped to x' through the lines of sight crossing the axis. The image $S(x')$ of a light source being on the flux surface poked by the axis at x'' gives $T(x', x = x'')$.

Definition (2) suggests the way to calculate the transfer function $T(x', x)$, since the choice of the emissivity $I(x) = \delta(x - x'')$ gives $S(x') = T(x', x'')$, where x'' scans all possible values of x. For a given measurement configuration, the $T(x', x)$ transfer function of observation can indeed be calculated by simulating the observation of virtual light sources on the x'' flux surfaces for a whole range of x'' values, as it is illustrated in Fig. 1.

On Fig. 2, two transfer functions are contour plotted, illustrating the features of the deviation from an *ideal measurement* that would give a $\delta(x' - x)$-like transfer function fully centered upon the diagonal. Fig. 2a corresponds to an unfavorable set-up, when the lines of sight are quite far from tangential to the flux surfaces, in contrast to Fig. 2b. A horizontal cut of the former transfer function is a wide Gaussian-like curve, showing that a detector segment in a given x' position collects the information from a broad range of spatial coordinates x. The closer the lines of sight to tangential are to the flux surfaces at the beam position, the more local the measurement is.
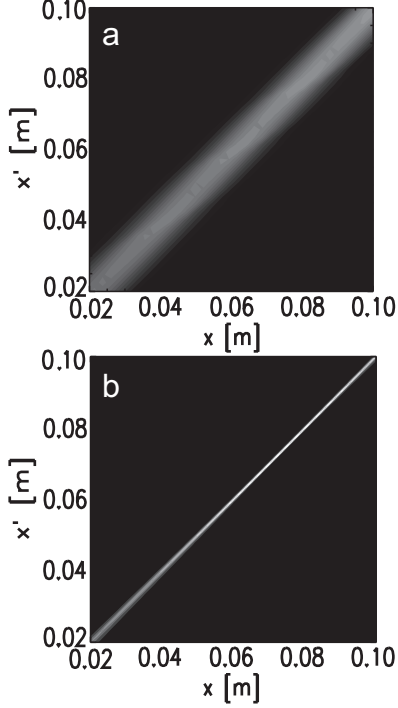
Figure 2: Simulated transfer functions. The observation angle is high (a) or small (b).

The effect caused by the broadening of the transfer function, due to finite thickness of the beam, on the measured light profile and the corresponding density profile is illustrated for a quite unfavorable but still realistic case. The angle between the lines of sight and the flux surfaces, which we call *observation angle*, is approximately $45°$ on average at the beam position. The observation system is located 0.45 m far from the observed region. A Gaussian current distribution beam with full width at half maximum of 1.2 cm is injected into a high density plasma with pedestal. For this case the transfer function is similar to Fig. 2a, and the corresponding light profiles are presented in Fig. 3a-b. The emissivity distribution of an infinitesimally fine beam $I(x)$ would give the best measurement of the electron density on the beam axis, up to the accuracy of the density profile reconstruction method. This strictly local measurement is referred as *ideal* (solid line). In reality we measure a light profile (*measured*, dotted line) affected by the finite beam width, that is smoothed compared to the *ideal*. Before the density calculation, the measured profile is corrected to the spatially slowly varying geometrical efficiency factor giving the profile labeled as "calibrated" (dashed line). Note that the density reconstruction does not require

8

the absolute value of the emissivity, only the shape of the light profile.

The relative differences from the *ideal* profile with respect to the maximum intensity are plotted in Fig. 3b. Note that while the relative difference between the *ideal* and the *calibrated* profiles is 5 % at $x = 5$ cm, the maximum relative error of the density profile calculated from the calibrated light profile is 23 % within the same range as it is shown on Fig. 3c-d, where the corresponding density profiles are plotted together with the differences from the density profile used as input to the light profile calculations (*original*, dash-dotted line). The density profiles are calculated by the Absolut code [6]. The *corrected* (long dashed line) curves show the result of the *emission reconstruction* correction method, which is introduced in the next section.
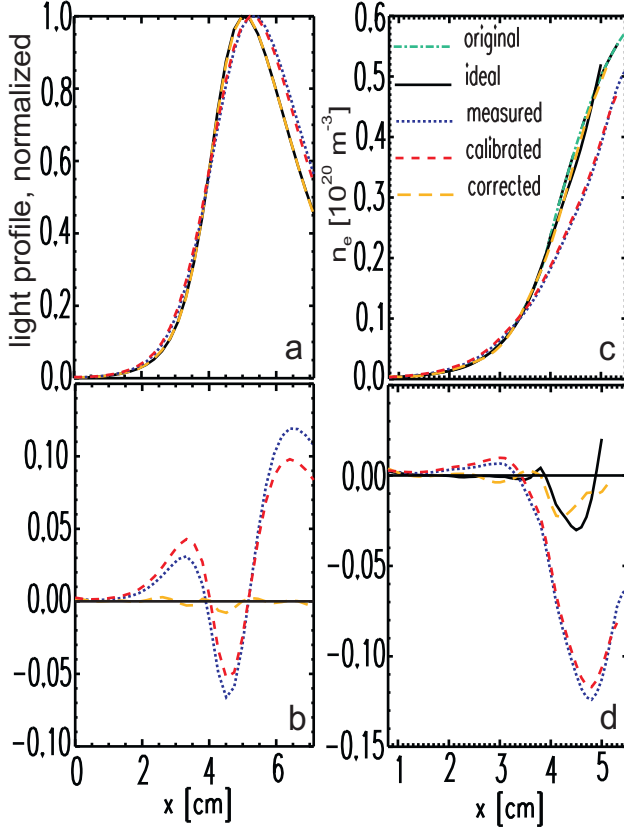

Figure 3: Li-BES, COMPASS; outboard mid-plane injection observed from the in-board side top port. a – light profiles, b – differences from the *ideal* light profile, c – density profiles, d – differences from the *original* density profile.

4 Emission reconstruction

A de-convolution based method can be introduced for the correction of undesired smoothing effect due to the observation of a finite width beam addressed in the previous section. The method uses the properties of the beam evolution and the transfer function, and assumes that the plasma parameters are flux functions in the spatial scale of the beam width.

Two essential aspects determine the characteristics of the transfer function: On one hand, the fact that we integrate over a range of flux surfaces, as the line of sight goes through the beam, gives the extradiagonal elements if we represent the discretized functions as a matrix. On the other hand, the geometrical efficiency of detection, the main factor of which is the variation of the solid angle of observation along the beam, is responsible for the slow trends in the magnitude. The latter effect would remain even if we used an ideal beam, and thus it is usually taken into consideration in the 1D calculations.

The two above effects are nearly independent of each other, thus the transfer function can be separated

$$
S(x') = \int T(x', x)I(x)\mathrm{d}x \approx \int p(x)t(x', x)I(x)\mathrm{d}x \approx \tag{3}
$$
$$
\approx \int p(x)\tau(x' - x)I(x)\mathrm{d}x \approx p(x')\int \tau(x' - x)I(x)\mathrm{d}x,
$$

where in the first step, we introduced a slowly varying function $p(x)$ containing the geometrical efficiency factors, and the effect of the integration along the lines of sight is represented by $t(x, x')$. Note that in an ideal measurement, $t(x', x) = \delta(x' - x)$. In the second step, $t(x', x)$ is approximated by a convolution kernel $\tau(x' - x)$. This approximation means that the width of $t(x', x)$ is independent of x, being valid if the observation angle does not vary too much in the observed region. In the third step we used that $p(x)$ is a slowly varying function of x compared to $\tau(x' - x)$.

We introduce the *calibrated* light profile $S'(x') = S(x')/p(x')$, where the geometrical efficiency along the beam axis $p(x')$ is calculated by the simulation, but otherwise an

easily measurable quantity. The convolution kernel can be estimated by $\tau(x' - x) = T(x' - x + x_c, x_c)/p(x_c)$ with x_c being in the middle of the x range relevant from the density profile calculation point of view.

In order to invert a convolution, it is expedient to consider the problem in Fourier space. The convolution theorem gives

$$\hat{S}'(k) = \hat{\tau}(k)\hat{I}(k), \tag{4}$$

where "hat" denotes the Fourier transform of a function. If $\hat{\tau} \neq 0$ for any k the problem would be solved, since then the inverse Fourier transform of

$$\hat{I}(k) = \hat{S}'(k)/\hat{\tau}(k) \tag{5}$$

would give the desired solution $I(x)$. In reality, $\tau(x' - x)$ has a typical scale length, which is comparable to the beam width. Therefore, there is a finite k, above which $\hat{\tau}(k)$ drops rapidly, which we denote by k_τ. Division by such a $\hat{\tau}(k)$ according to (5) would amplify high wave number part of the noise present in the spectrum of the measured light profile. The spectrum of the measured light profile also decays exponentially due to the finite spontaneous decay time of the atomic states, but reaches the noise level at a frequency k_S intrinsically much lower than k_τ. To get around the problem we can zero out $1/\hat{\tau}(k)$ above k_S before the multiplication with $\hat{S}'(k)$.

Typical wave number spectra of the emission reconstruction are plotted on Fig. 4. The corrected light profile spectrum plotted by dashed line can be expressed as $\Theta(k_S - k)\hat{S}'/\hat{\tau}$, where $\Theta(k)$ is the Heaviside function. It decays rapidly with a slope determined by the spontaneous transition frequency of the observed transition, while the calibrated spectrum $\hat{S}'$ (solid line) decays even somewhat faster due to the decaying $\hat{\tau}$ *transmission* of the observation in wave number space (dotted line). The de-convolution function $\Theta(k_S - k)/\hat{\tau}$ is plotted with dash-dotted line.

As we will see, there are measurement configurations and plasma parameters profiles
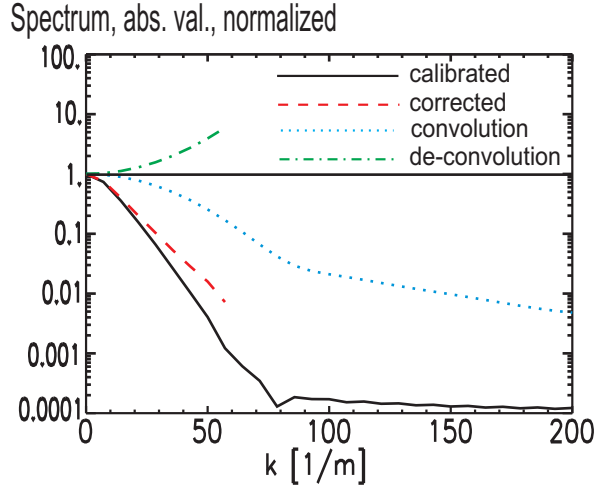
Figure 4: Wave number spectra of functions involved in emission reconstruction.

when the smoothing effect of the observation does not cause significant error in the reconstructed density profile, however the quantification of the transmission of the system is still of importance, if the radial wave number spectrum of a BES fluctuation measurement is to be investigated. The smallest measurable spatial scale is limited by the effect of the finite lifetime of the ι atomic state, although, there is a considerable part of the wave number spectrum that can be underestimated by not considering the transmission.

5   Realistic numerical tests

In the present section, the effects of the finite beam width on the light profile and the corresponding density profile are investigated in simulations for the COMPASS and the TEXTOR tokamaks. The undesired smoothing of the light profile due to the integration along the lines of sight through different stages of beam evolution is corrected by the emission reconstruction method introduced in the previous section.

The COMPASS simulations are based on the plasma parameter profiles of the $1.2 \cdot 10^{20}$ m^{-3} central electron density H-mode shot #30866 (156 ms). The 40 keV Li/Na beam is injected in the outboard mid-plane, while the observation system is located in the same poloidal position at the high field side (HFS) or middle top ports. The latter set-up, which is the planned one for the COMPASS reinstalled at Prague recently, is

shown in an output file of RENATE, Fig. 5, where the emissivity of the Li beam is contour plotted; additionally, the magnetic geometry and the lines of sight together with the vacuum chamber are also indicated.

A lower density ($3.2 \cdot 10^{19}$ m^{-3}) shot #107242 (2730 ms) is taken from the TEXTOR circular tokamak, where the 35 keV Li beam is observed from a low field side (LFS) top port through a periscope system with quite high observation angle. The TEXTOR Li-BES set-up [13] is shown in Fig. 6. The corresponding sodium calculations are based on similar measurement geometry and the assumption of a 40 keV Na beam.
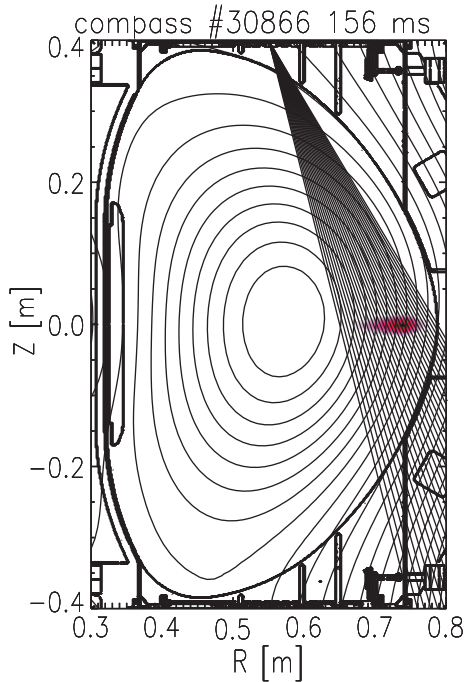

Figure 5: Investigated configuration and simulated beam emissivity, COMPASS.

There are two aspects of the measurement playing important role in the enhancement of the finite beam width effects: the observation angle and the scale length of the light profile compared to the beam width. The first one is mainly determined by the measurement geometry apart from the case of significantly variable magnetic geometry devices. In certain cases, the location of the observation system can not be chosen to give optimal observation angle, because of technical constraints, such as on the TEXTOR set-up [13]. The second aspect depends on the beam width, which is determined by the ion optics, and also on the plasma parameter profiles and the beam material determining
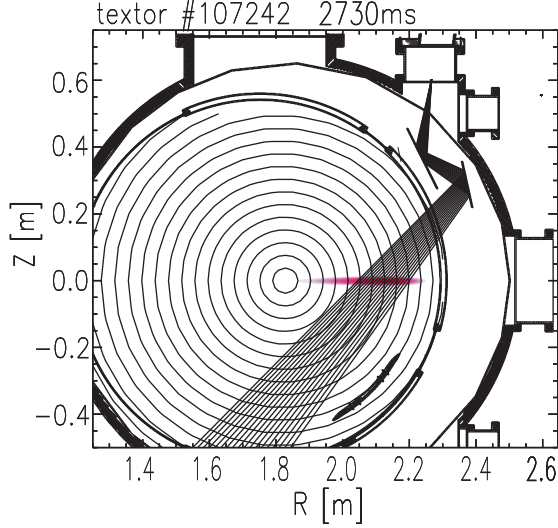
Figure 6: Investigated configuration and simulated beam emissivity, TEXTOR.

the beam evolution.

The finite beam width effects on the light profile were discussed in the end of Sec. 3 and were illustrated on Fig. 3 showing a simulated Li-BES measurement on the COM-PASS tokamak with LFS observation. In this case, besides the unfavorable observation direction, the relatively steep density gradient also enhances the smoothing of the light profile, since the characteristic length scale of the light profile– the distance between the point where the beam enters the plasma and the light profile maximum – is only 5 cm, comparable to the beam width. The varying geometrical efficiency has smaller effect according to the *measured* and *calibrated* curves on 3b. This difference is even more pronounced in the reconstructed density profiles calculated by the Absolut code, as seen on Fig. 3c-d. Here, the differences are measured with respect to the *original* density profile that was the input for the light profile calculations, which enables to show the accuracy of the density calculation method, as even the *ideal* density profile has a certain error. The *calibrated* density profile is also smoothed compared to the *ideal*, significantly underestimating the density at the pedestal region, however, its relative systematic error is approximately four times larger than that of the corresponding light profile.

The result of the emission reconstruction calculation from the *measured* light profile and the corresponding density profile is plotted with long-dashed line (*corrected*). The

14

relative error of the *corrected* profile is only 1 % at the maximum in contrast to the 10 % maximum error in the *calibrated* one, or 5 % in the region of interest from density profile calculation point of view. This error in the *corrected* profile causes 6 % error in the density profile, which is the same magnitude as the error due to the imperfections of the density calculation.

According to the current plans the observation system of the COMPASS BES will be installed into the middle top port, as in Fig. 5, which is more favorable, since the angle between the flux surfaces and the lines of sight is only $\sim 25\,^\circ$ on average, however the systematic error for the same parameters is still not negligible, more than 15 %; see Fig. 7. The error in the *calibrated* light profile follows the same pattern as in the previous case, however the overestimation outside the $4-5$ cm range is considerably lower. The *calibrated* light profile has more than four times higher error then the *corrected* one, and the improvement for the density profiles is a factor of three, although as the *ideal* density profile shows, the improvement is limited again by the accuracy of the density calculation.

As we pointed out not only the observation direction, but the scale length of the light profile is also important in the finite beam effects of a density profile measurement. The scale length is affected on the one hand by the plasma parameter distributions along the beam line, mainly the electron density distribution and slightly by the beam energy, the temperature profile and impurity concentrations, and on the other hand the beam material. In the TEXTOR test case the density gradients are much lower than for the COMPASS case, giving three times longer light profile scale length, much higher than the beam width (see Fig. 6). Although the observation angle is $50\,^\circ$ the finite beam width effects are negligible.

However, the emission reconstruction method can potentially be used for the density profile measurement during a two-dimensional fluctuation measurement. The beam scans in the poloidal direction (at 400 kHz on TEXTOR) in order to give good poloidal velocity resolution of the turbulent structures, while the concurrent profile measurement has a much lower sampling rate, thus the different beam positions are seen simultaneously. The
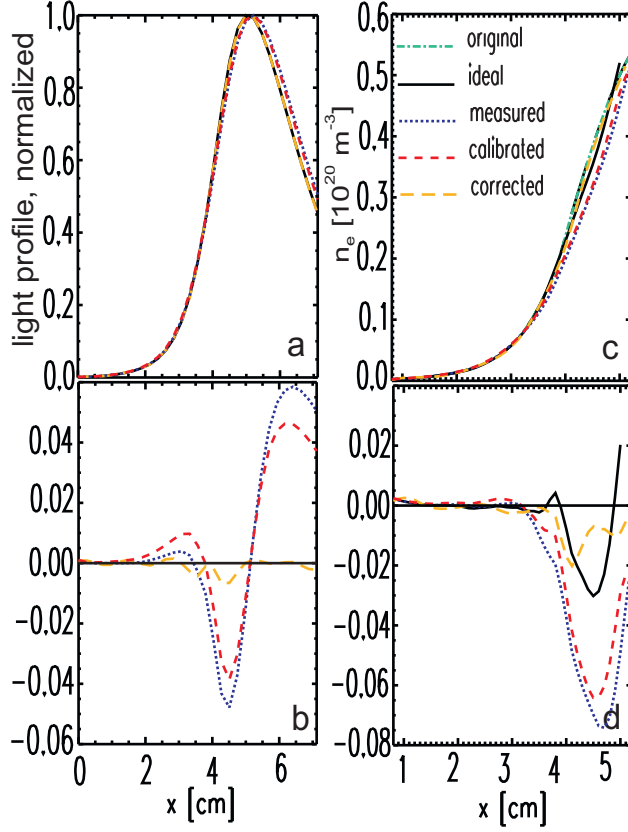
Figure 7: Light profile differences; Li-BES, COMPASS, observation from the middle top port.

configuration is equivalent with the observation of only one, quite thick beam ($\sim$ 5 cm), which clearly gives non-negligible finite beam width effects.

The effect of the beam material is illustrated by Na beam simulations, in Fig. 8 and 9. For a smaller ionization energy atom, such as Na, the light profile becomes shorter for the same plasma parameter distributions, which enhances the finite beam width effects. For middle top port observation COMPASS case using Na beam, shown in Fig. 8, the overestimation of the light profile is more than two times higher than with Li beam (7), while the error of the *corrected* light profile is the same in both cases. In the TEXTOR case, shown on Fig. 9, similar trend can be seen. For Li beam the systematic error of the *measured* profile was clearly dominated by the geometrical efficiency effects, but for Na the contribution of the finite beam width effects gives the half of this error.
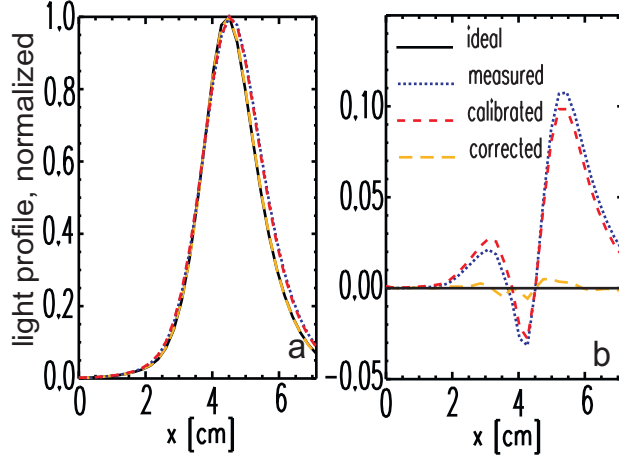
Figure 8: Na-BES, COMPASS tokamak; a – light profiles, b – differences from the *ideal* light profile
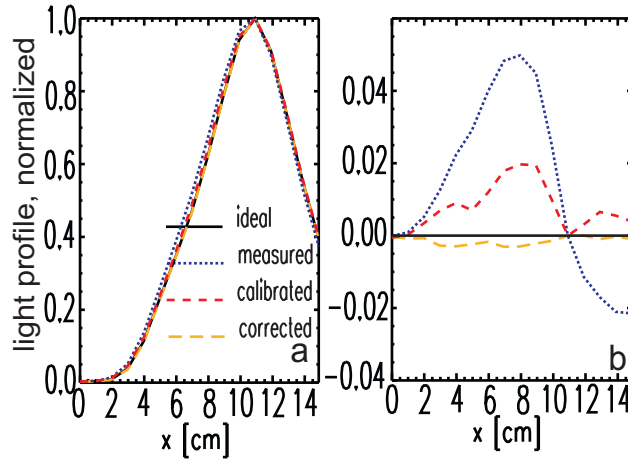

Figure 9: Na-BES, TEXTOR tokamak; a – light profiles, b – differences from the *ideal* light profile

6 Error estimation for Li-BES measurements

After having investigated the characteristics of the error caused by the finite beam width on typical simulated measurements of the COMPASS and TEXTOR tokamaks, it is instructive to quantitatively measure the different factors affecting the error, on the basis of which it can be estimated for different measurements and configurations. In this chapter we focus only on measurements using lithium as beam material, which is the most common for diagnostic purpose beams.

Assuming that the evolution of plasma parameters follow the flux surfaces, for given plasma parameters, we expect the error to be proportional to the typical width of the
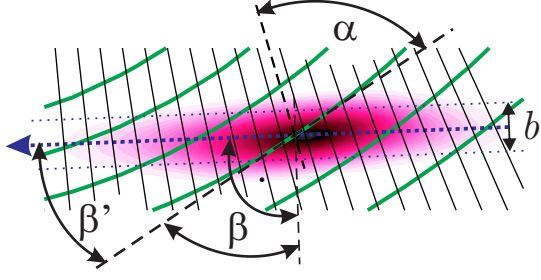
Figure 10: The relevant parameters characterizing the observation geometry. b – the full width at half maximum of the beam, α – observation angle, β' – the angle between the beam axis and the flux surfaces, $\beta = \pi/2 - \beta'$. Thick dotted line: beam axis, thick solid curves – flux surfaces, thin solid lines: lines of sight.

range of flux surfaces we integrate through along the line of sight. This width can be estimated as $b\,|\sin(\alpha)/\cos(\alpha-\beta)|$, where b is the full width at half maximum of the beam, α is the observation angle and $\beta = \pi/2 - \beta'$, if β' is the angle between the beam axis and the flux surfaces (see Fig. 10). The trigonometric expression gives no error, when the lines of sight are tangential to the flux surfaces, and diverges as they become parallel to the beam axis; although, the latter configuration is quite unnatural. Here, we note that the first assumption of the paragraph breaks down if β' is too small. If the axis is perpendicular to the flux surfaces on average, the expression reduces to $b\,|\tan\alpha|$. These angles are average values over a range along the beam relevant to the measurement.

Experience with several simulations for a wide range of plasma parameter profiles showed that the most important parameter affecting the magnitude of the systematic error is the electron density at the maximum of the light profile n_{e*}, and that the dependence of the maximum relative error in electron density on this parameter is approximately linear. The maximum relative error usually occurs in the vicinity of the light profile maximum, and due to the fact, that the light profile smoothing effect of the observation mainly lowers the logarithmic derivative of the light profile, the error always appears as an underestimation of the electron density.

Investigating the effect of the electron temperature on the error, we found that the relative variation of the error for different temperature profiles is comparable to the relative variation of the quantity $\int n_e(x)\tilde{a}_{2p,2s}(T(x))dx$, where we integrate from the point
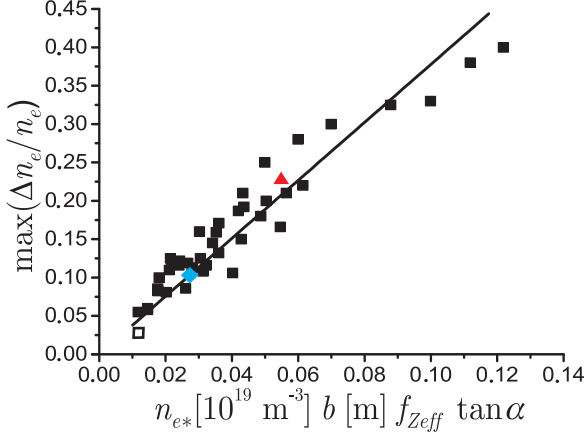
18

Figure 11: Comparison of the maximum relative error in electron density with the model given in Eq. 6 (solid line) for different measurement configurations and plasma parameter profiles. The cyan diamond corresponds to the configuration of Fig. 5, the white square to Fig. 6, while the red triangle is the simulation of Fig. 3.

where the beam enters the plasma to the maximum of the light profile. This variation is negligibly small for an experimentally relevant range of SOL/edge temperatures, therefore can be neglected. Finally the error shows a relatively weak linear dependence on Z_{eff}. Thus, the maximum relative error can be estimated as

$$max(|\Delta n_e/n_e|) = C n_{e*} b f_{Zeff} \left| \sin(\alpha)/\cos(\alpha - \beta) \right|, \qquad (6)$$

where $f_{Zeff} = 0.068 \, Z_{eff} + 0.9$, n_{e*} is given in 10^{19} m^{-3}, b is in m and the constant C is found by linear fitting to be 3.8.

In Fig. 11 maximum relative errors are plotted against $n_{e*} b f_{Zeff} |\tan(\alpha)|$ for a various plasma parameter profiles, observation angles and beam widths; in these cases the beam axis is chosen to be perpendicular to the flux surfaces. The errors are calculated for the densities corresponding to the *calibrated* light profiles, accordingly contain only the effects due to the finite beam width. The considerable deviation of the errors with respect to the estimation indicated by the line is partly due to the finite accuracy of the density calculation method, but profile effects of the plasma parameter distributions, that would be difficult to parameterize, also play important role.

Equation (6) predicts 21 % relative error for the COMPASS case shown in Fig. 3,

where we found 23 %, and 4.5 % for the simulated TEXTOR measurement in Fig. 6, which is indeed lower than the achieved accuracy of the density calculation for that case. The formula can be used to give a rough estimate to the error expected for a measurement configuration, however, it is not capable of giving accurate implications to the error of a certain measurement, and in particular, can not be used for correction of the error; for that, one has to resort to the comprehensive simulation of the BES measurement (e.g. using the RENATE code).

7 Conclusions

In the present paper a de-convolution based correction method of alkali BES density profile measurements has been presented and demonstrated in simulated measurements on the TEXTOR and the COMPASS tokamak using the actual/planned BES configuration respectively. We found that in set-ups, where the line of sight is far from tangential to the flux surfaces at the beam position, the observation can cause an undesired smoothing of the light profile, which results in an underestimation of the reconstructed density profile, up to $15 - 20$ % for realistic cases. The systematic error caused by the finite beam width is larger for higher electron densities and for sodium or beam materials with even lower binding energies.

The systematic error investigated here caused by the integration along the lines of sight is important, since it causes information losses on the fine structure of the profile, and leads to the underestimation of the pedestal density gradient, degrading the capabilities of the BES measurement in very important fields such as investigation of L–H transitions.

A general estimation of the maximal relative error in electron density is presented, reflecting that the error is proportional to the electron density at the light profile maximum and shows a linear dependence on Z_{eff}, while its temperature dependence is negligible for experimentally relevant temperature profiles. Furthermore, it is proportional to the beam width and to the tangent of the average angle between the flux surfaces and the lines of sight. The maximum relative error regularly occurs near to the light profile maximum

20

and always appears as an underestimation of the electron density.

The *transfer function of the observation*, playing crucial role in the *emission recon-struction*, is calculated by the RENATE alkali BES simulation code. It takes the finite beam width and all basic properties of the measurement into account, assuming that the plasma parameters are flux functions on the scale of the beam width. Separating the transfer function into a slowly varying part due to geometrical efficiency effects and a convolution kernel describing the smoothing of the light profile, the problem can be reduced to a simple algebraic equation in wave number space.

The de-convolution method gives a good estimate of the emissivity on the beam axis from the measured light profile, so that the level of the remaining error due to the observation is in the order of the accuracy of the density profile reconstruction algorithm (in our case the Absolut code [6]). The method allows the use of the one dimensional density calculation methods even for the configurations where the finite width of the beam is not negligible.

Acknowledgements

References

[1] K. McCormick, S. Fiedler, G. Kocsis, J. Schweinzer, S. Zoletnik, Fus. Eng. and Des. **34-35**, 125-134 (1997).

[2] S. Zoletnik, M. Anton, M. Endler, S. Fiedler, M. Hirsch, K. McCormick, J. Schweinzer, Phys. Plasmas **6**, 4239-4247 (1999).

[3] B. Schweer, Fusion Sci. Tech. **49**, 404-411 (2006).

[4] K. Igenbergs, J. Schweinzer, I. Bray, D. Bridi, F. Aumayr, Atomic Data and Nuclear Data Tables **94**, 981-1014 (2008).

[5] E. Wolfrum, J. Schweinzer, D. Bridi, K. Igenbergs, J. Kamleitner, F. Aumayr, J. Nucl. Mat. **390-391**, 1110-1113 (2009).

[6] J. Schweinzer, E. Wolfrum, F. Aumayr, M. Pökl, H. Winter, A. Unterreiter, Plasma Phys. Control. Fusion **34**, 1173-1183 (1992).

[7] R. Fischer, E. Wolfrum, J. Schweinzer and the ASDEX Upgrade Team, Plasma Phys. Control. Fusion **50**, 085009 (2008).

[8] T. Oishi, S. Kado, M. Yoshinuma, K. Ida, S. Tanaka, S. Okamura, J. Plasma Fusion Res. SERIES **6**, 449-452 (2004).

[9] S. Zoletnik, G. Petravich, A. Bence, M. Berta, S. Fiedler, K. McCormick, J. Schweinzer, Rev. Sci. Instrum. **76**, 073504 (2005).

[10] R. P. Schorn, E. Hintz, D. Rusbüldt, F. Aumayr, M. Schneider, E. Unterreiter, H. Winter, App. Phys. B **52**, 71-78 (1991).

[11] Z. A. Pietrzyk, P. Breger, D. D. R. Summers, Plasma Phys. Control. Fusion **35**, 1725-1744 (1993).

[12] K. Nakamura, H. Iguchi, M. Ueda, Z. Narihiro, A. Shimizu, T. Morisaki, M. Isobe, C. Takahashi, S. Nishimura, c. Suzuki, Y. Yoshimura, K. Nagaoka, T. Minami, M. Yoshinuma, K. Ida, S. Okamura, K. Matsuoka, Rev. Sci. Instrum. **76**, 013504 (2005).

[13] G. Anda, G. Petravich, D. Dunai, J. Sárközi, S. Zoletnik, B. Schweer, I. G. Kiss, T. Baross, *35th EPS Conference on Controlled Fusion and Plasma Physics* P-5.076 (2008).

[14] R. Pánek, O. Bilyková, V. Fuchs, M. Hron, P. Chráska, P. Pavlo, J. Stöckel, J. Urban, V. Weinzettl, J. Zajac, F. Žáček, Czechoslovak Journal of Physics **56**, B125-B137 (2006).

[15] J. Schweinzer, R. Brandenburg, I. Bray, R. Hoekstra, F. Aumayr, R. K. Janev H. P. Winter, Atomic Data and Nuclear Data Tables **72**, 239-273 (1999)

[16] D. Wutte, R. K. Janev, F. Aumayr, M. Schneider, J. Schweinzer, J. J. Smith, H. P. Winter, Atomic Data and Nuclear Data Tables **65**, 155-180 (1997)

[17] J. Schweinzer, D. Wutte, HP. Winter, J. Phys. B **27**, 137-153 (1994)

[18] http://physics.nist.gov/PhysRefData/ASD/

Original sources:

Lithium: A. N. Zaidel, V. K. Prokofev, S. M. Raiskii, V. A. Slavnyi, and E. Y. Schreider, Tables Of Spectral Lines, 3rd Edition, IFI/Plenum, New York (1970),

Sodium: P. Risberg, Ark. Fys. **10**, 583 (1956).